Packet-Error-Rate Analysis Using Markov Models of the Signal-to-Interference Ratio for Mobile Packet Systems

Kazuhiko Fukawa, *Member, IEEE*, Hiroshi Suzuki, *Member, IEEE*, and Yumiko Tateishi

***Abstract*—To analyze the packet error rate (PER) of interference-limited mobile packet systems, in this paper, two Markov models of the time-varying signal-to-interference ratio (SIR) are derived over frequency-selective fading channels. The two Markov models are first-order two-state for the following two cases: 1) infinitesimal interval and 2) finite-time interval. The state and state transition probabilities are obtained from both the level crossing rate and average outage duration of the fluctuating SIR. The PER is analytically derived using the Markov model in the case of a finite time interval, and the analysis can be applied not only to cellular communication systems but to ad hoc mobile networks as well. The analytical results are exact when the average powers of both the desired and interfering signal components are equal for all paths but include an approximation in the other cases. The analytical results of the PER agree well with the results that were obtained by computer simulations. It is also shown that the PER characteristics of cellular systems and of ad hoc networks are almost the same.**

***Index Terms*—Ad hoc network, average outage duration (AOD), cellular system, level crossing rate (LCR), Markov model, packet error rate (PER), signal-to-interference ratio (SIR).**

I. Introduction

THE PACKET error rate (PER) is one of the most important factors for characterizing packet transmissions on mobile radio channels. To evaluate the PER, link-level simulations that involve upper layer protocols have been conducted, but they require a great deal of computational time [1]. One method to reduce the computational time is to apply Markov models that represent the link-level process [1]–[6].

A first-order Markov model is a very good fit for slow flat-fading channels [5]. In particular, the two-state first-order Markov model that was described in [6] is very simple but accurate to some extent. This model divides the received signal-to-noise ratio (SNR) into two states; it assumes that a packet is correctly received when the SNR continues to be greater than a threshold for the entire packet. To improve the accuracy, the two-state model is extended to the finite-state Markov model (FSMC), which partitions the SNR into a finite number of states [7]–[10].

The conventional Markov models assume flat-fading channels and focus on the SNR. In wideband cellular systems, however, frequency-selective fading should be considered. In addition, cochannel interference more severely affects the throughput performance than noise does, because the received power remains almost constant due to the wide frequency band, and major systems such as direct spread code-division multiple-access (DS-CDMA) systems are interference limited. Thus, a PER analysis based on the signal-to-interference ratio (SIR) over frequency-selective fading channels is preferable to that based on the SNR over flat-fading channels. Although many papers have analyzed such SIRs and both the level crossing rate (LCR) and average outage duration (AOD) of the SIR [11]–[14], few papers have studied Markov models of SIRs [15]–[17]. The Markov models of the SIR that were discussed in [15] and [16] are applied to DS-CDMA systems under closed-loop power control, and the state and state transition probabilities are not analytically but approximately derived by data-fitting methods such as the context tree pruning algorithm. On the other hand, the transition probabilities of the Markov model that was described in [17] are determined by the transmit-power-control error probability. Note that the state and state transition probabilities of the Markov models that were discussed in [15]–[17] are not analytically derived from channel propagation models. It is also noteworthy that resource allocation under the interference-limited condition that was described in [18] uses the FSMC of the SNR.

With the aim of evaluating the PER of interference-limited packet transmission, this paper theoretically derives Markov models of the time-varying SIR over frequency-selective fading channels, which are quite different from the aforementioned Markov models. In the derivation, we assume only the open-loop transmit power control, which cannot sufficiently track the fluctuating SIR. The derived Markov models are also applicable to the ad hoc network, where both transmitters and receivers move around (this mobility is referred to as "double mobility") [19]. The state and state transition probabilities are obtained from both the LCR and AOD of the SIR. Furthermore, the PER is evaluated from one of the Markov models for a finite time interval. Note that these items were presented in part in [20], which assumed that both the average powers of desired signal components and of interfering signal components are equal for all paths, whereas in this paper, we have made no such

Manuscript received August 18, 2011; revised February 8, 2012; accepted March 26, 2012. Date of publication May 2, 2012; date of current version July 10, 2012. The review of this paper was coordinated by Prof. W. A. Hamouda.

K. Fukawa and H. Suzuki are with the Department of Communications and Integrated Systems, Tokyo Institute of Technology, Tokyo 152-8550, Japan (e-mail: fukawa@radio.ss.titech.ac.jp; suzuki@radio.ss.titech.ac.jp).

Y. Tateishi is with the Department of Computational Intelligence and Systems Science, Tokyo Institute of Technology, Kanagawa 226-8503, Japan.

Digital Object Identifier 10.1109/TVT.2012.2197231

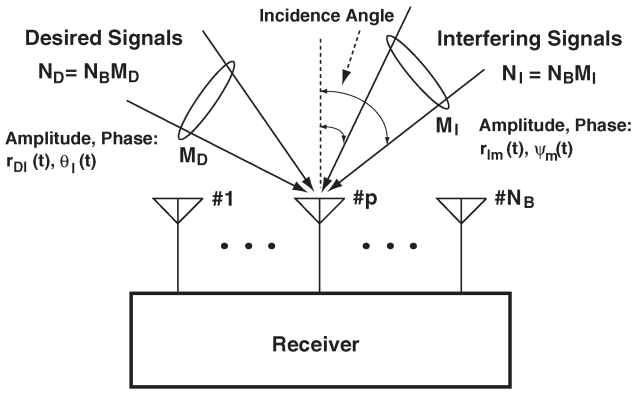

Fig. 1. Signal model.

assumptions. In addition, this paper provides a detailed signal model, discusses a relation between the LCR of the SIR and the SNR, and compares the analytical results of the PER with the results that were obtained by computer simulations, which did not appear in [20].

The rest of this paper is organized as follows. Section II presents the signal model that was used in this paper. The double mobility and the LCR and AOD of the SIR are also discussed. Note that the LCR and AOD of the SIR are derived in more general cases, including the ad hoc network, which have not been analyzed in [11]–[14]. Section III describes the following two new Markov models of the SIR: 1) an infinitesimal-time-interval model and 2) a finite-time-interval model. The PER is evaluated using the latter model. Finally, concluding remarks are given in Section IV.

II. Signal-to-Interference Ratio Characteristics

A. Signal Model

This paper considers an interference-limited packet transmission system in which desired packets always suffer from interfering signals. Furthermore, it is assumed that only the open-loop transmit power control is employed and the fluctuating SIR is not tracked. Even under such conditions, the packets can correctly be received, provided that the value of the instantaneous SIR exceeds a threshold.

As shown in Fig. 1, it is assumed that the desired and interfering signals are composed of $N_D(\geq 1)$ and $N_I(\geq 1)$ propagation paths, respectively. The desired signals from a single transmitter are received at different incidence angles with different temporal delays and are assumed to be statistically independent of each other. Because this paper considers only the non-line-of-sight condition, complex envelopes of the paths are assumed to be complex Gaussian variables with zero mean. With regard to the paths of the interfering signals, the same assumptions are made, except for the assumption that relates to the single transmitter, and the interfering signal components are assumed to be statistically independent of the desired ones.

The aforementioned signal model can be applied to both cellular and ad hoc mobile network systems. First, let us consider the cellular system. In the frequency-division multiple access (FDMA) and time-division multiple access (TDMA) cellular systems, the interfering signals are received from transmitters in different cells, which reuse the same carrier frequency. Thus, N_I also depends on the carrier frequency reuse pattern other than the channel conditions. In DS-CDMA cellular systems, the interfering signals are received from transmitters in all cells, because they share the same carrier frequency. Therefore, N_I of DS-CDMA systems is much larger than FDMA and TDMA systems. Because DS-CDMA is of the despreading type and the powers of interfering signal components can be reduced, the power of one interfering signal is much less than FDMA and TDMA.

Let us assume that the receiver is equipped with $N_B(\geq 1)$ antennas. A signal that was received at the pth $(1 \leq p \leq N_B)$ antenna $y_p(t)$ can be expressed as

$$y_p(t) = \sum_{l=1+(p-1)M_D}^{pM_D} r_{Dl}(t) \cos\left[2\pi f_c t + \theta_l(t)\right] + \sum_{m=1+(p-1)M_I}^{pM_I} r_{Im}(t) \cos\left[2\pi f_c t + \psi_m(t)\right] + n_p(t) \quad (1)$$

where f_c is the carrier frequency, and $n_p(t)$ represents the additive Gaussian noise. M_D and M_I are the numbers of paths per antenna of the desired and interfering signals, respectively. Thus, $N_D = N_B M_D$, and $N_I = N_B M_I$. $r_{Dl}(t)$ and $\theta_l(t)$ are the envelope and random phase, respectively, of a desired signal component that follows the lth $(1 \leq l \leq N_D)$ path. Let $b_{Dl,0}$ denote the average power of $r_{Dl}(t)$. Hence, $b_{Dl,0} = \langle r_{Dl}^2(t) \rangle / 2$, where $\langle\, \rangle$ denotes the statistical expectation operator. In addition, $r_{Im}(t)$ and $\psi_m(t)$ are the envelope and random phase, respectively, of an interfering signal component that follows the mth $(1 \leq m \leq N_I)$ path. Let $b_{Im,0}$ denote the average power of $r_{Im}(t)$; thus, $b_{Im,0} = \langle r_{Im}^2(t) \rangle / 2$.

To obtain the SIR, we discuss several signal detection methods for alleviating the degradation of transmission performance due to fading channels. Such methods are based on the maximal-ratio-combining principle. For example, the FDMA for narrowband systems employs multiple antennas and performs maximal ratio combining to obtain the space diversity effect. TDMA and DS-CDMA for wideband systems perform maximum-likelihood sequence estimation (MLSE) and RAKE, respectively, to obtain the path diversity effect. These techniques enable the desired signal components to efficiently be received and optimally be combined.

Let $\lambda_p(t)$ denote the SIR of the received signal $y_p(t)$. When the desired signal components can optimally be combined by RAKE or equalization such as MLSE and the power of the interference can be ensemble averaged with respect to $\psi_m(t)$, $\lambda_p(t)$ is given by

$$\lambda_p(t) = \sum_{l=1+(p-1)M_D}^{pM_D} r_{Dl}^2(t) \Bigg/ \sum_{m=1+(p-1)M_I}^{pM_I} r_{Im}^2(t). \quad (2)$$

Note that the derivation of the numerator in (2) uses the frequency selectivity of the channels that each propagation path has a different temporal delay, where differences of the delays are comparatively large. Thus, the paths of the desired signals can optimally be combined by RAKE or MLSE. It is also

noteworthy that the denominator in (2) is derived by averaging the square of the second term of (1) with respect to $\psi_m(t)$.

Furthermore, the total SIR of the reception is defined as follows. When maximal ratio combining is employed and the interfering signals can be regarded as Gaussian noise, the SIR $\lambda_C(t)$ of diversity combining can be expressed as [21]

$$\lambda_C(t) = \sum_{p=1}^{N_B} \lambda_p(t). \tag{3}$$

The analysis of $\lambda_C(t)$ is very complicated. To simplify the analysis, this paper discusses its lower bound, which is denoted by $\lambda(t)$, i.e.,

$$\lambda_C(t) \geq \lambda(t) \tag{4}$$

where $\lambda(t)$ is defined as

$$\lambda(t) = \frac{r_D^2(t)}{r_I^2(t)} \tag{5}$$

and $r_D(t)$ and $r_I(t)$ are the envelopes of the total desired signal given by (6), shown below, and the total interference given by (7), shown below, respectively

$$r_D(t) = \sqrt{\sum_{l=1}^{N_D} r_{Dl}^2(t)} \tag{6}$$

$$r_I(t) = \sqrt{\sum_{m=1}^{N_I} r_{Im}^2(t)}. \tag{7}$$

To prove that $\lambda(t)$ is the lower bound of $\lambda_C(t)$, $\lambda(t)$ as defined in (5) is rewritten as

$$\lambda(t) = \sum_{p=1}^{N_B} \beta_p(t)\lambda_p(t) \quad \beta_p(t) = \frac{\sum_{m=1+(p-1)M_I}^{pM_I} r_{Im}^2(t)}{r_I^2(t)}. \tag{8}$$

The inequality $0 \leq \beta_b(t) \leq 1$, (3), and (8) determine the lower bound. Note that the SIR $\lambda(t)$ defined in (5) can be used not only for flat fading but for frequency-selective fading channels as well, and it is exactly equal to the total SIR when $N_B = 1$.

In addition, note that this paper does not consider temporal fluctuations of $b_{Dl,0}$ and $b_{Im,0}$ due to log-normal shadowing, because the time length of packet reception is very short such that the shadowing can be considered unchanged. In addition, even when the time length of packet reception is long, the open-loop transmit power control can track the shadowing and keep $b_{Dl,0}$ and $b_{Im,0}$ constant. Nevertheless, the SIR fluctuates due to the Doppler effect.

In the following discussion, the following two typical cases of $b_{Dl,0}$ and $b_{Im,0}$ are considered.

1. Equal Average Power (EAP), where $b_{Dl,0}$ and $b_{Im,0}$ are constant independent of the indices l and m, i.e., $b_{Dl,0} = b_{D0}, 1 \leq l \leq N_D$ and $b_{Im,0} = b_{I0}, 1 \leq m \leq N_I$;
2. Unequal Average Power (UAP), where $b_{Dl_1,0} \neq b_{Dl_2,0}$ for $l_1 \neq l_2$ and $b_{Im_1,0} \neq b_{Im_2,0}$ for $m_1 \neq m_2$, where $1 \leq l_1, l_2 \leq N_D$, and $1 \leq m_1, m_2 \leq N_I$.

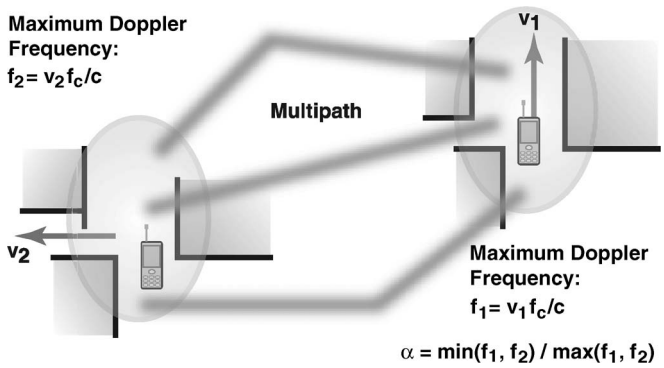

Fig. 2. Ad hoc network.

B. Double Mobility

To establish the ad hoc network conditions, let us introduce the power density spectra of the signal components that are affected by the double mobility [19]. As shown in Fig. 2, both the receiver and transmitter move around in an ad hoc network. Let v_1 and v_2 denote the velocities of the terminals, which are measured on the ground. f_1 and f_2 are the maximum Doppler frequencies and are defined as $v_1 f_c/c$ and $v_2 f_c/c$, respectively, where c is the velocity of light. Then, the power density spectra $S(f)$ of the desired and interfering signal components are given by

$$S(f) = S_1(f) \otimes S_2(f) \tag{9}$$

where $\otimes$ denotes the convolution operation, and $S_i(f)$, $i = 1$, 2, are defined as [22]

$$\begin{cases} S_i(f) \propto \frac{1}{\pi\sqrt{f_i^2 - f^2}}, & -f_i \leq f \leq f_i \\ S_i(f) = 0, & \text{otherwise.} \end{cases} \tag{10}$$

Note that these power density spectra are derived under the following assumptions; the incidence and departure angles of the propagation paths are uniformly distributed. Therefore, directions of the velocity vectors of the receiver and the transmitter are irrelevant to the double mobility, and thus, f_1 and f_2 have sufficient information on the double mobility.

Let $\rho(\tau)$, $\rho_1(\tau)$, and $\rho_2(\tau)$ be the inverse Fourier transforms of $S(f)$, $S_1(f)$, and $S_2(f)$, respectively. $\rho(\tau)$ is equivalent to the autocorrelation function of the signal component and is expressed as

$$\rho(\tau) = \rho_1(\tau)\rho_2(\tau) \propto J_0(2\pi f_1 \tau) J_0(2\pi f_2 \tau) \tag{11}$$

where $J_0(x)$ is the zeroth-order modified Bessel function of the first kind [22].

Let $r(t)$ be used to represent either $r_{Dl}(t)$ or $r_{Im}(t)$. Then, the average powers of $r(t)$ and $\dot{r}(t)$ can be written as $b_0 = \langle r^2(t) \rangle/2$ and $b_2 = \langle \dot{r}^2(t) \rangle$. Using $\rho(\tau)$, b_0 and b_2 can be expressed as [22]

$$b_0 = \rho(0)/2, \quad b_2 = \ddot{\rho}(0). \tag{12}$$

When $\rho(\tau)$ of (11) is expanded in a Taylor series, the coefficients of τ^0 and τ^2 are equal to $\rho(0)$ and $\ddot{\rho}(0)/2$, respectively.

Thus, the ratio b_2/b_0 yields

$$\frac{b_2}{b_0} = 2\pi^2(1+\alpha^2)f_D^2 \tag{13}$$

where $f_D = \max(f_1, f_2)$. α denotes *the degree of double mobility* and is defined as $\alpha = \min(f_1, f_2)/\max(f_1, f_2)$ [19]. Thus, α depends on the difference between the velocities of the receiver and the transmitter, and it ranges from 0 to 1. For example, α is equal to 0 for cellular mobile communication systems, because the base station is fixed, and $\min(f_1, f_2) = 0$. On the other hand, when both the receiver and the transmitter move at the same speed, α is equal to 1.

C. LCR

The LCR N_c of the SIR is defined as the expectation value of the rate at which $\lambda(t)$ crosses the threshold λ_{th} in the positive direction [11], [12]. If the level crossing occurs during an infinitesimal time interval $[t, t+dt]$, then the following conditions are satisfied:

$$\begin{cases} \lambda(t) < \lambda_{th} \\ \lambda(t+dt) > \lambda_{th}. \end{cases} \tag{14}$$

Using (5), (14) can be rewritten as

$$r_D(t) < \lambda_{th}^{1/2} r_I(t) \tag{15}$$

$$r_D(t+dt) > \lambda_{th}^{1/2} r_I(t+dt). \tag{16}$$

Because dt is an infinitesimal time interval, the Taylor expansion of (16) yields

$$r_D(t) + \dot{r}_D(t)dt > \lambda_{th}^{1/2} r_I(t) + \lambda_{th}^{1/2}\dot{r}_I(t)dt. \tag{17}$$

Thus, the probability $P_c[\lambda_{th}|t, t+dt]$ that $\lambda(t)$ crosses λ_{th} in the positive direction during the time interval $[t, t+dt]$ is given by

$$P_c[\lambda_{th}|t, t+dt] = \int_{-\infty}^{\infty} d\dot{r}_D \int_{-\infty}^{\lambda_{th}^{-1/2}\dot{r}_D} d\dot{r}_I \int_0^{\infty} dr_I \times \int_{\lambda_{th}^{1/2} r_I + \lambda_{th}^{1/2}\dot{r}_I dt - \dot{r}_D dt}^{\lambda_{th}^{1/2} r_I} dr_D p(r_D, \dot{r}_D, r_I, \dot{r}_I) \tag{18}$$

where $r_D(t)$, $\dot{r}_I(t)$, $r_I(t)$, and $\dot{r}_I(t)$ are abbreviated as r_D, $\dot{r}_D$, r_I, and $\dot{r}_I$. $p(r_D, \dot{r}_D, r_I, \dot{r}_I)$ is the joint probability density function. Because dt is infinitesimal, (18) can be rewritten as

$$P_c[\lambda_{th}|t, t+dt] = dt \int_{-\infty}^{\infty} d\dot{r}_D \int_{-\infty}^{\lambda_{th}^{-1/2}\dot{r}_D} d\dot{r}_I \times \int_0^{\infty} dr_I \left(\dot{r}_D - \lambda_{th}^{1/2}\dot{r}_I\right) p\left(\lambda_{th}^{1/2} r_I, \dot{r}_D, r_I, \dot{r}_I\right). \tag{19}$$

When the unit of time is divided into $M(=1/dt)$ infinitesimal time intervals, the crossing occurs at most only once during each time interval. Thus, N_c can be expressed as

$$N_c = \sum_{k=0}^{M-1} P_c\left[\lambda_{th}|t+kdt, t+(k+1)dt\right]. \tag{20}$$

Because r_D, $\dot{r}_D$, r_I, and $\dot{r}_I$ are stationary stochastic processes, $P_c[\lambda_{th}|t+kdt, t+(k+1)dt]$ is independent of k and is given by (19). Hence, (20) can be rewritten as

$$N_c = \int_{-\infty}^{\infty} d\dot{r}_D \int_{-\infty}^{\lambda_{th}^{-1/2}\dot{r}_D} d\dot{r}_I \times \int_0^{\infty} dr_I \left(\dot{r}_D - \lambda_{th}^{1/2}\dot{r}_I\right) p\left(\lambda_{th}^{1/2} r_I, \dot{r}_D, r_I, \dot{r}_I\right). \tag{21}$$

$p(r_D, \dot{r}_D, r_I, \dot{r}_I)$ on the right-hand side of (21) is derived in Appendix A and is given by

$$p(r_D, \dot{r}_D, r_I, \dot{r}_I) = p_D(r_D)p_D(\dot{r}_D)p_I(r_I)p_I(\dot{r}_I) \tag{22}$$

$$p_D(r_D) = \begin{cases} \frac{2}{(N_D-1)!}\frac{r_D^{2N_D-1}}{(2b_{D0})^{N_D}} \\ \times \exp\left(-\frac{r_D^2}{2b_{D0}}\right), & \text{for EAP} \\ \sum_{l=1}^{N_D} \frac{\pi_{Dl} r_D}{b_{Dl,0}} \exp\left(-\frac{r_D^2}{2b_{Dl,0}}\right), & \text{for UAP} \end{cases} \tag{23}$$

$$p_D(\dot{r}_D) = \begin{cases} \frac{1}{\sqrt{2\pi b_{D2}}} \exp\left(-\frac{\dot{r}_D^2}{2b_{D2}}\right), & \text{for EAP} \\ \frac{1}{\sqrt{2\pi\dot{\sigma}_D^2}} \exp\left(-\frac{\dot{r}_D^2}{2\dot{\sigma}_D^2}\right), & \text{for UAP} \end{cases} \tag{24}$$

$$p_I(r_I) = \begin{cases} \frac{2}{(N_I-1)!}\frac{r_I^{2N_I-1}}{(2b_{I0})^{N_I}} \exp\left(-\frac{r_I^2}{2b_{I0}}\right), & \text{for EAP} \\ \sum_{m=1}^{N_I} \frac{\pi_{Im} r_I}{b_{Im,0}} \exp\left(-\frac{r_I^2}{2b_{Im,0}}\right), & \text{for UAP} \end{cases} \tag{25}$$

$$p_I(\dot{r}_I) = \begin{cases} \frac{1}{\sqrt{2\pi b_{I2}}} \exp\left(-\frac{\dot{r}_I^2}{2b_{I2}}\right), & \text{for EAP} \\ \frac{1}{\sqrt{2\pi\dot{\sigma}_I^2}} \exp\left(-\frac{\dot{r}_I^2}{2\dot{\sigma}_I^2}\right), & \text{for UAP} \end{cases} \tag{26}$$

where

$$\pi_{Dl} = \prod_{k=1, k\neq l}^{N_D} \frac{b_{Dl,0}}{b_{Dl,0} - b_{Dk,0}} \tag{27}$$

$$\left\langle \dot{r}_D^2 \right\rangle = \begin{cases} b_{D2} = 2\pi^2(1+\alpha^2)f_{DD}^2 b_{D0}, & \text{for EAP} \\ \dot{\sigma}_D^2 = \frac{2\pi^2(1+\alpha^2)f_{DD}^2 \sum_{l=1}^{N_D} b_{Dl,0}^2}{\sum_{l=1}^{N_D} b_{Dl,0}}, & \text{for UAP} \end{cases} \tag{28}$$

$$\pi_{Im} = \prod_{k=1, k\neq m}^{N_I} \frac{b_{Im,0}}{b_{Im,0} - b_{Ik,0}} \tag{29}$$

$$\left\langle \dot{r}_I^2 \right\rangle = \begin{cases} b_{I2} = 2\pi^2(1+\alpha^2)f_{DI}^2 b_{I0}, & \text{for EAP} \\ \dot{\sigma}_I^2 = \frac{2\pi^2(1+\alpha^2)f_{DI}^2 \sum_{m=1}^{N_I} b_{Im,0}^2}{\sum_{m=1}^{N_I} b_{Im,0}}, & \text{for UAP.} \end{cases} \tag{30}$$

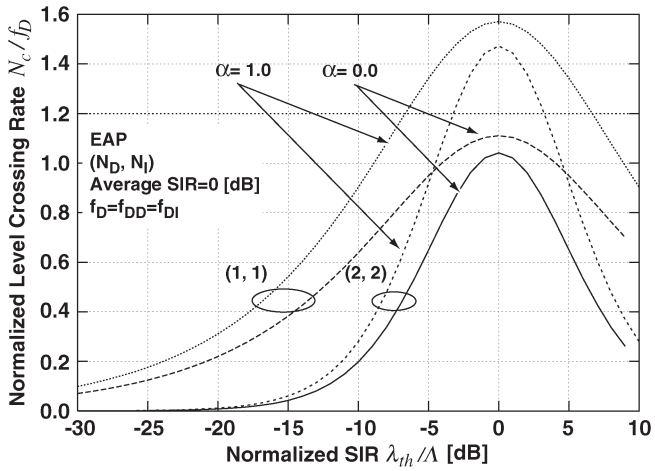

Fig. 3. LCR for the EAP condition: N_c.

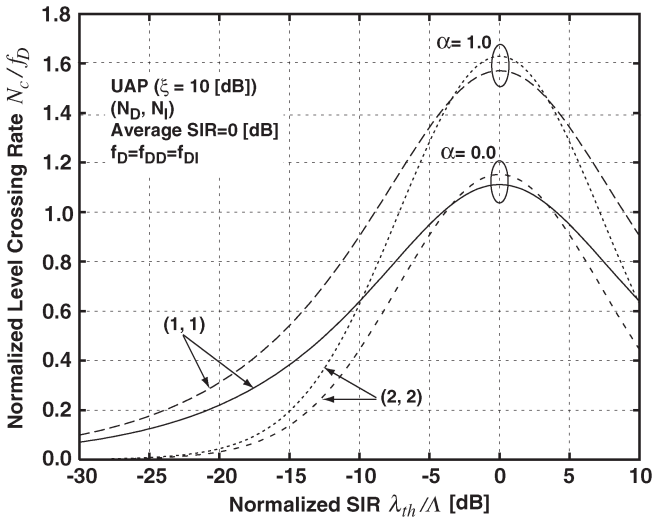

Fig. 4. LCR for the UAP condition ($\xi = 10$ dB): N_c.

In the aforementioned equations, f_{DD} and f_{DI} are the maximum Doppler frequencies of the desired and interfering signals, respectively. Note that the derivation of (28) and (30) requires the use of (13) and (24) and (26) are approximate forms in the case of UAP.

Substituting (22) into (21) yields

$$N_c = AB \tag{31}$$

$$A = \int_{-\infty}^{\infty} d\dot{r}_D p_D(\dot{r}_D) \int_{-\infty}^{\lambda_{th}^{-1/2}\dot{r}_D} d\dot{r}_I \left(\dot{r}_D - \lambda_{th}^{1/2}\dot{r}_I\right) p_I(\dot{r}_I) \tag{32}$$

$$B = \int_{0}^{\infty} dr_I p_D\left(\lambda_{th}^{1/2} r_I\right) p_I(r_I). \tag{33}$$

A and B are calculated in Appendix B, and N_c is given by

$$N_c = \begin{cases} \dfrac{(2N_D+2N_I-3)!!}{2^{N_D+N_I-1}(N_D-1)!(N_I-1)!} \\ \times \dfrac{\lambda_{th}^{\frac{2N_D-1}{2}} b_{D0}^{\frac{2N_I-1}{2}} b_{I0}^{\frac{2N_D-1}{2}} b_{t2}^{1/2}}{b_{t0}^{(2N_D+2N_I-1)/2}}, & \text{for EAP} \\ \dfrac{\lambda_{th}^{1/2}\left(\dot{\sigma}_D^2+\lambda_{th}\dot{\sigma}_I^2\right)^{1/2}}{2} \\ \times \sum_{l=1}^{N_D}\sum_{m=1}^{N_I} \dfrac{\pi_{Dl}\pi_{Im}(b_{Dl,0}b_{Im,0})^{1/2}}{(b_{Dl,0}+\lambda_{th}b_{Im,0})^{3/2}}, & \text{for UAP} \end{cases} \tag{34}$$

where $(2N-1)!!$ denotes $(2N-1)(2N-3)\cdots 1$. b_{t0} and b_{t2} are defined as

$$b_{t0} = b_{D0} + \lambda_{th} b_{I0} \tag{35}$$

$$b_{t2} = b_{D2} + \lambda_{th} b_{I2}. \tag{36}$$

Note that, when $f_D = f_{DD} = f_{DI}$, b_{t2} is given by

$$b_{t2} = 2\pi^2(1+\alpha^2) f_D^2 b_{t0}. \tag{37}$$

Fig. 3 shows the effect of the threshold λ_{th} on the LCR N_c when the average SIR $\Lambda = (N_D b_{D0})/(N_I b_{I0}) = 0$ dB under the EAP condition. The peak of N_c appears at $\lambda_{th} = \Lambda$, and N_c increases with α, because the fading more rapidly varies with larger α values. It is also observed that N_c decreases with N_D and N_I due to the diversity effect.

Fig. 4 also shows how λ_{th} affects N_c when the average SIR $\Lambda = \sum_{l=1}^{N_D} b_{Dl,0} / \sum_{m=1}^{N_I} b_{Im,0} = 0$ dB under the UAP condition. The path power ratio (in decibels) ξ is defined as $\xi = 10\log_{10}(b_{Dl,0}/b_{Dl+1,0})$, where $1 \le l \le N_D - 1$. ξ was set to 10 dB. In Figs. 3 and 4, it can be observed that, when $N_D = N_I = 1$, N_c under the EAP condition is equal to N_c under the UAP condition, because these two conditions are equivalent. When $N_D = N_I = 2$, the results in Fig. 3 are equal to the results with $\xi = 0$ dB under the UAP condition, because $\xi = 0$ dB corresponds to EAP. Therefore, in Figs. 3 and 4, it can also be observed that N_c increases with ξ when $N_D = N_I = 2$. This case is because an increase in ξ removes the diversity effect.

Another LCR $\tilde{N}_c$, i.e., the expected rate where $\lambda(t)$ crosses λ_{th} in the negative direction, can similarly be derived as in N_c. As expected, $\tilde{N}_c$ equals N_c.

D. AOD

The AOD $\overline{\tau}$ is defined as the average duration for which the SIR $\lambda(t)$ remains less than λ_{th}. $\overline{\tau}$ is also a critical measure for characterizing a fading channel.

During a very long time interval T_o, the level crossing occurs $N_c T_o$ times. When the duration of the ith outage is denoted by τ_i, the AOD $\overline{\tau}$ is given by

$$\overline{\tau} = \frac{\sum_{m=1}^{M} \tau_m}{T_o N_c} = \frac{P_l}{N_c} \tag{38}$$

$$P_l = \frac{\sum_{m=1}^{M} \tau_m}{T_o}. \tag{39}$$

If the process is ergodic, the time average P_l is equal to the ensemble average, and it is equal to the probability that $r_D(t) < \lambda_{th}^{1/2} r_I(t)$. Therefore

$$P_l = \int_{0}^{\infty} dr_I p_I(r_I) \int_{0}^{\lambda_{th}^{1/2} r_I} dr_D p_D(r_D) = 1 - P_u \tag{40}$$

where P_u is the probability that $r_D(t) \ge \lambda_{th}^{1/2} r_I(t)$.

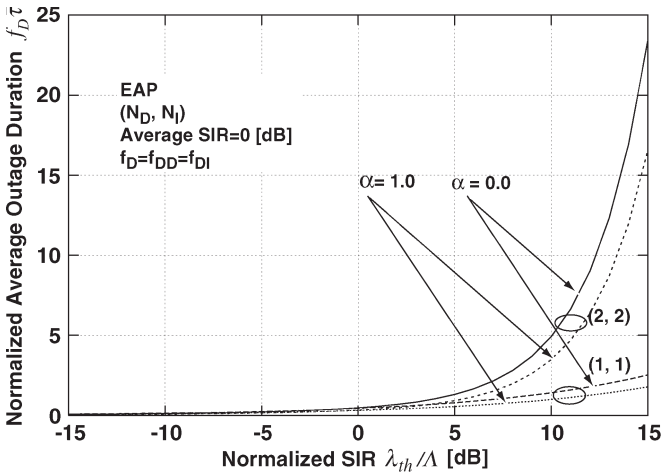

Fig. 5. AOD for the EAP condition: $\overline{\tau}$.

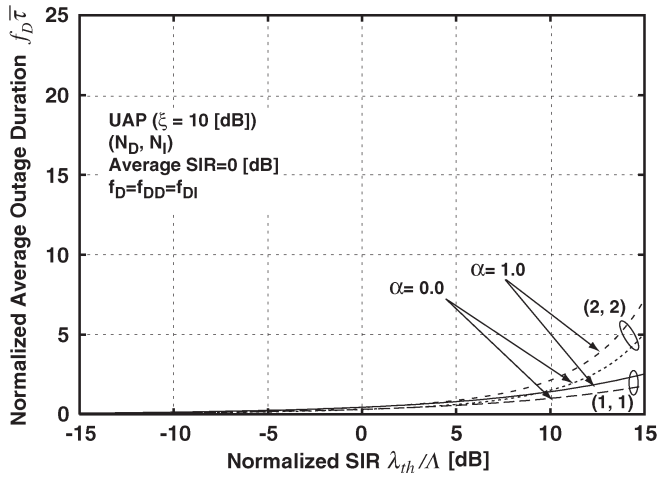

Fig. 6. AOD for the UAP condition ($\xi = 10$ dB): $\overline{\tau}$.

P_u is derived in Appendix C and given by

$$P_u = \begin{cases} \left(\frac{b_{D0}}{b_{t0}}\right)^{N_I} \sum_{k=0}^{N_D-1} \binom{N_D+N_I-k-2}{N_I-1} \\ \times \left(\frac{\lambda_{th} b_{I0}}{b_{t0}}\right)^{N_D-k-1}, & \text{for EAP} \\ \sum_{l=1}^{N_D} \sum_{m=1}^{N_I} \frac{\pi_{Dl}\pi_{Im} b_{Dl,0}}{b_{Dl,0}+\lambda_{th} b_{Im,0}}, & \text{for UAP.} \end{cases} \quad (41)$$

Thus, $\overline{\tau}$ can be obtained by substituting (34), (40), and (41) into (38).

Fig. 5 shows the effect of λ_{th} on the AOD $\overline{\tau}$ when the average SIR Λ is equal to 0 dB and the equality $f_D = f_{DD} = f_{DI}$ holds under the EAP condition. $\overline{\tau}$ increases with λ_{th} and decreases with α, because the fading more rapidly varies at larger α values. It is also observed that $\overline{\tau}$ increases with N_D and N_I due to the diversity effect.

Fig. 6 also shows how λ_{th} affects $\overline{\tau}$ when the average SIR Λ is equal to 0 dB and the equality $f_D = f_{DD} = f_{DI}$ holds under the UAP condition. ξ was set to 10 dB. In Figs. 5 and 6, it is observed that, when $N_D = N_I = 1$, $\overline{\tau}$ under the UAP condition is equal to $\overline{\tau}$ under the EAP condition, because these two conditions are equivalent. When $N_D = N_I = 2$, the results in Fig. 5 are equal to the results with $\xi = 0$ dB under the UAP condition, because $\xi = 0$ dB corresponds to EAP. Therefore, in Figs. 5 and 6 it can also be observed that $\overline{\tau}$ decreases with ξ when $N_D = N_I = 2$. This case is because, when ξ increases, the diversity effect is lost.

E. Relationship Between the LCRs of SIR and SNR

The aforementioned LCR of the SIR is equivalent to the LCR of the SNR if the number of interfering signals is infinite when the sum of the average interference powers is fixed. To prove this case, let us consider the conditions of EAP as

$$\begin{cases} N_D = 1, \alpha = 0 \\ b_{I0} = b_I/N_I \\ b_{I2} = 0. \end{cases} \quad (42)$$

In this case, N_c of (34) becomes

$$N_c = \lim_{N_I\to\infty} \frac{(2N_I-1)!!}{2^{N_I}(N_I-1)!} \frac{(\lambda_{th} b_I/N_I)^{1/2} b_{D0}^{N_I-1/2} b_{D2}^{1/2}}{(b_{D0}+\lambda_{th} b_I/N_I)^{N_I+1/2}}. \quad (43)$$

Substituting (28) for $\alpha = 0$ into (43) gives

$$\begin{aligned} N_c &= 2^{1/2}\pi f_{DD} \left(\frac{\lambda_{th} b_I}{b_{D0}}\right)^{1/2} \\ &\quad \times \lim_{N_I\to\infty} \frac{(2N_I-1)!!}{2^{N_I}(N_I-1)! N_I^{1/2}} \left(1+\frac{\lambda_{th} b_I}{b_{D0} N_I}\right)^{-N_I-1/2} \\ &= 2^{1/2}\pi f_{DD} \left(\frac{\lambda_{th} b_I}{b_{D0}}\right)^{1/2} \lim_{N_I\to\infty} \frac{(2N_I)! N_I^{1/2}}{(2^{N_I} N_I!)^2} \\ &\quad \times \lim_{N_I\to\infty} \left[\left(1+\frac{\lambda_{th} b_I}{b_{D0} N_I}\right)^{N_I}\right]^{-1} \left(1+\frac{\lambda_{th} b_I}{b_{D0} N_I}\right)^{-1/2} \\ &= \sqrt{2\pi} f_{DD} \left(\frac{\lambda_{th} b_I}{b_{D0}}\right)^{1/2} \exp\left(-\frac{\lambda_{th} b_I}{b_{D0}}\right) \end{aligned} \quad (44)$$

where the following formulas are used:

$$\lim_{N_I\to\infty} \left[\left(1+\frac{a}{N_I}\right)^{N_I}\right]^{-1} = \exp(-a) \quad (45)$$

$$\lim_{N_I\to\infty} \frac{(2N_I)! N_I^{1/2}}{(2^{N_I} N_I!)^2} = \pi^{-1/2}. \quad (46)$$

Note that (44) is a well-known formula for the LCR of the SNR [22]. Therefore, the expression for the SIR is an extension of the LCR for the SNR. The infinite number of interfering signals causes sphere hardening in the N_I-D vector space, which means that the instantaneous power of the total interference does not fluctuate.

III. Markov Model of Signal-to-Interference Ratio

A. Infinitesimal Time-Interval Model

Let us construct a new Markov model of the SIR for the infinitesimal period dt. The model is illustrated in Fig. 7(a); the propagation conditions are classified into two states. The states U and L represent the channel conditions for which the SIR is greater than and smaller than or equal to λ_{th} at a certain time t, respectively. These states are observed at kdt, where k

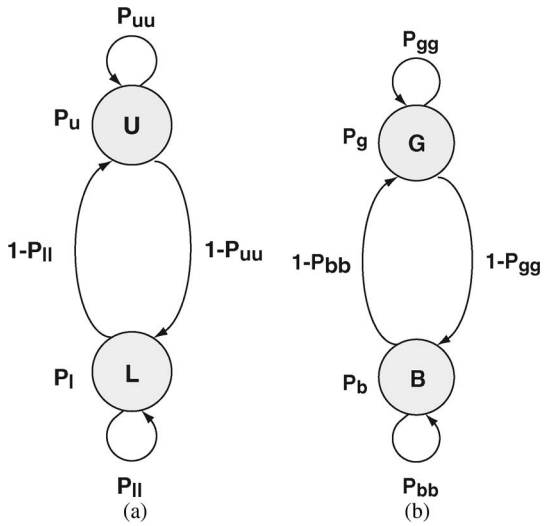

Fig. 7. Markov models. (a) Infinitesimal-time-interval model. (b) Finite-time-interval model.

is an integer. The period dt is set very short such that the state transitions can occur at most only once during the time interval dt. The probabilities of these states, i.e., P_u and P_l, are given by (41) and (40), respectively. Because the SIR $\lambda(t)$ undergoes a stationary stochastic process, the state transition probabilities satisfy the following equation:

$$P_u + P_l = 1 \quad P_u(1 - P_{uu}) = P_l(1 - P_{ll}) \tag{47}$$

where P_{uu} and P_{ll} are the transition probabilities from state U to state U and from state L to state L, respectively. Based on (47) it is evident that P_{ll} can be obtained from P_u and P_{uu}. Therefore, P_{uu} is derived as follows.

When the SIR $\lambda(t)$ is greater than λ_{th} during the interval $[t, t + dt]$, the following equations hold:

$$r_D(t) > \lambda_{th}^{1/2} r_I(t) \tag{48}$$

$$r_D(t + dt) > \lambda_{th}^{1/2} r_I(t + dt). \tag{49}$$

To derive the probability P_o of (48) and (49), we consider another event that is given by

$$\begin{cases} r_D(t) > \lambda_{th}^{1/2} r_I(t) \\ r_D(t + dt) < \lambda_{th}^{1/2} r_I(t + dt). \end{cases} \tag{50}$$

The probability $\tilde{P}_c$ of this event and P_o satisfies

$$P_o + \tilde{P}_c = P_u. \tag{51}$$

Because $\tilde{P}_c$ is the probability that $\lambda(t)$ crosses λ_{th} in the negative direction during the time interval $[t, t + dt]$ and $\tilde{P}_c = \tilde{N}_c dt = N_c dt$, P_o can be written as

$$P_o = P_u - N_c dt. \tag{52}$$

Thus, the conditional probability P_{uu} of (49), given the occurrence of (48), is expressed as

$$P_{uu} = \frac{P_o}{P_u} = 1 - \frac{N_c}{P_u} dt. \tag{53}$$

B. Finite-Time-Interval Model

The model for an infinitesimal time interval can be extended to a model for a finite time interval T. The Markov model is illustrated in Fig. 7(b); states G and B represent the channel conditions for the SIR to remain greater than and smaller than or equal to λ_{th} during T, respectively. Because the SIR is a stationary stochastic process, the following equations hold:

$$P_g + P_b = 1 \quad P_g(1 - P_{gg}) = P_b(1 - P_{bb}) \tag{54}$$

where P_g and P_b are the probabilities of states G and B, respectively. P_{gg} and P_{bb} are the probabilities of the state transitions from state G to state G and from state B to state B, respectively. When P_g and P_{gg} are given, the other probabilities can be determined using (54) as follows:

$$P_b = 1 - P_g \quad P_{bb} = 1 - \frac{(1 - P_{gg})P_g}{(1 - P_g)}. \tag{55}$$

The aforementioned P_g and P_{gg} are derived as follows.

Because the SIR is a stationary stochastic process, P_{uu} is independent of time. Thus, the conditional probability P_{gg} that $\lambda(t)$ remains greater than λ_{th} during T, given that (48) has occurred, is expressed as

$$P_{gg} = \lim_{dt \to 0} (P_{uu})^{T/dt}. \tag{56}$$

Substituting (53) into (56) yields

$$P_{gg} = \lim_{dt \to 0} \left(1 - \frac{N_c T}{P_u} \cdot \frac{dt}{T}\right)^{T/dt} = \exp\left(-\frac{N_c T}{P_u}\right). \tag{57}$$

In addition, the probability P_g that $\lambda(t)$ remains greater than λ_{th} during T is equal to $P_u P_{gg}$ and is given by

$$P_g = P_u P_{gg} = P_u \exp\left(-\frac{N_c T}{P_u}\right). \tag{58}$$

Consequently, the state and transition probabilities of this Markov model can exactly be determined based on the signal model.

C. PER Definition and Numerical Examples

In general, a packet is identified as an error packet if at least one bit error is detected in the packet. The evaluation of the PER by conventional computer simulations therefore requires demodulating all bits in a packet, which involves significant computational time. To reduce this time, we assume that the packet error does not occur only if the SIR or its lower bound continues to be greater than λ_{th} for an entire packet, as shown in Fig. 8. With this assumption, the PER becomes equal to P_b derived for the aforementioned Markov model. The finite time interval T is set equal to the packet length, and the PER P_e is given by

$$P_e = P_b = 1 - P_g. \tag{59}$$

Fig. 9 shows a plot of the PER performance versus the normalized packet length $f_D T$ under the EAP condition, where

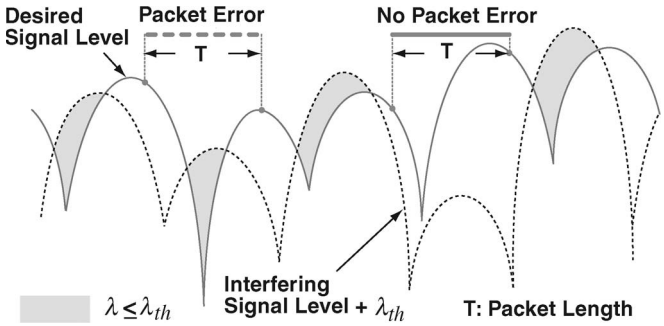

Fig. 8. Packet error.

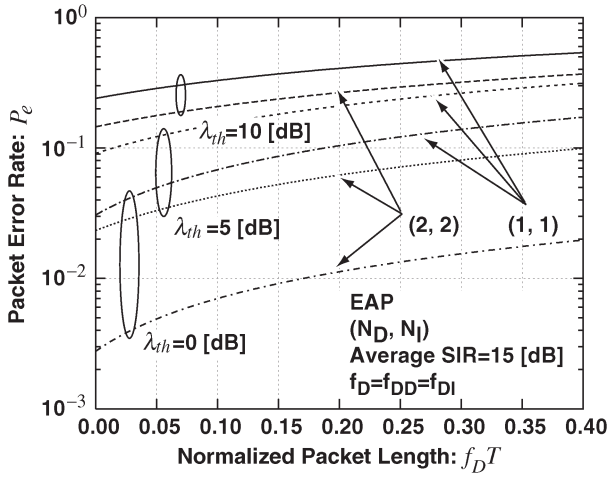

Fig. 9. PER for the EAP condition: P_e.

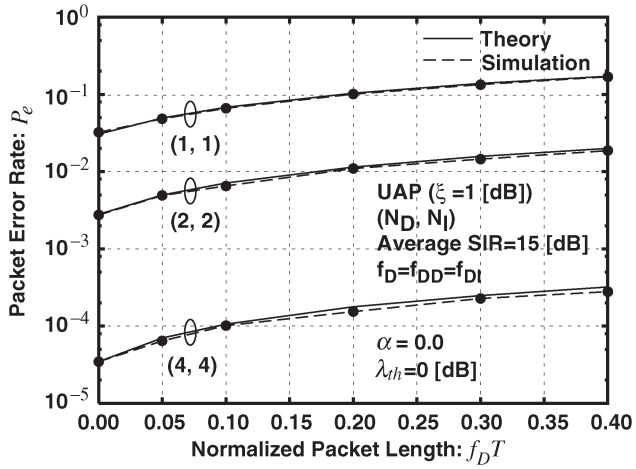

Fig. 10. PER for the cellular system ($\alpha = 0.0$) under the UAP condition ($\xi = 1$ dB): P_e.

$f_D = f_{DD} = f_{DI}$. The average SIR is set to 15 dB, and λ_{th} is specified as a parameter. As the packet length increases, the PER performance degrades due to the fading fluctuations. However, as N_D and N_I increase, the PER improves due to the diversity effect.

Figs. 10–13 compare the theoretical PER with the PER that was obtained by computer simulations under the UAP condition for $\xi = 1$ and 10 dB, respectively. This is the case where $f_D = f_{DD} = f_{DI}$, the average SIR is 15 dB, and λ_{th} is 0 dB.

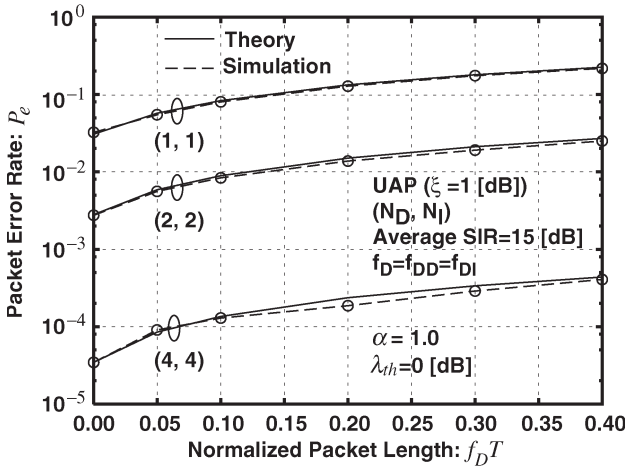

Fig. 11. PER for the ad hoc network ($\alpha = 1.0$) under the UAP condition ($\xi = 1$ dB): P_e.

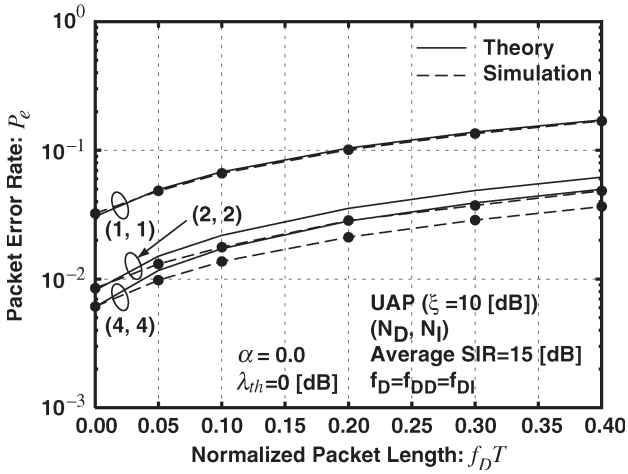

Fig. 12. PER for the cellular system ($\alpha = 0.0$) under the UAP condition ($\xi = 10$ dB): P_e.

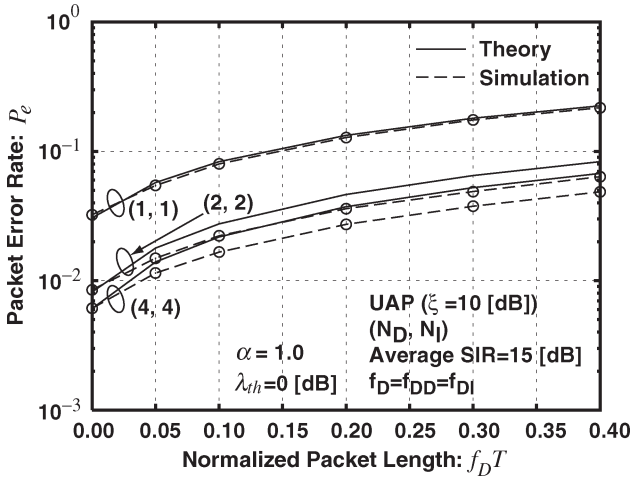

Fig. 13. PER for the ad hoc network ($\alpha = 1.0$) under the UAP condition ($\xi = 10$ dB): P_e.

$\alpha = 0$ in Figs. 10 and 12, whereas $\alpha = 1.0$ in Figs. 11 and 13. Therefore, Figs. 10 and 12 correspond to cellular systems, whereas Figs. 11 and 13 correspond to ad hoc networks. The simulations assume that the propagation paths are statistically

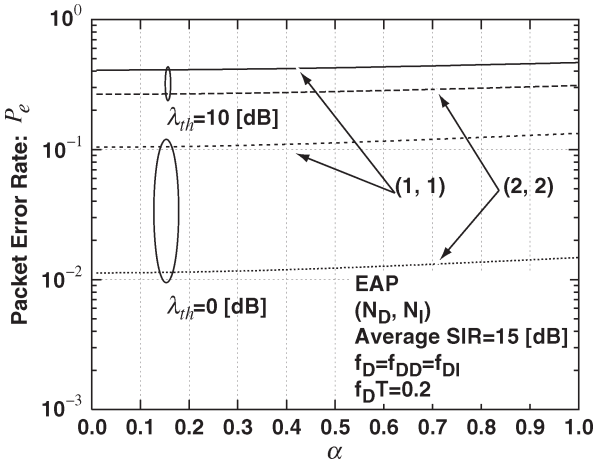

Fig. 14. PER in an ad hoc network for the EAP condition: P_e.

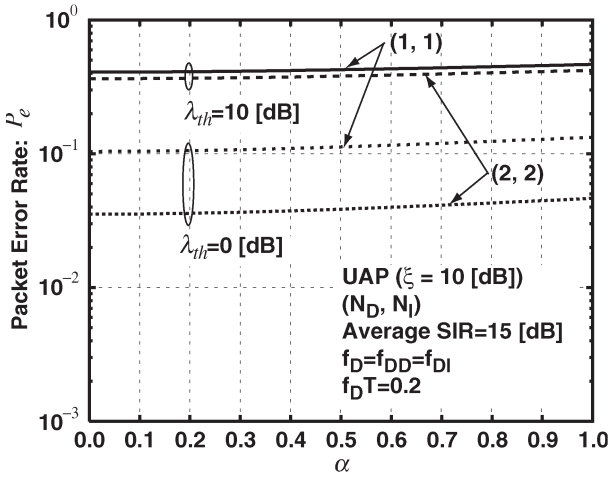

Fig. 15. PER in an ad hoc network for the UAP condition ($\xi = 10$ dB): P_e.

independent and follow the Rayleigh distribution. They were generated based on the Jakes model [22]. One run of the simulations investigates 100 consecutive packets, and each packet is composed of 200 symbols. The SIR is evaluated at each symbol timing and compared with λ_{th}. The number of simulation runs was set to 16×10^3. When $\xi = 1$ dB, the simulation results very well agree with the theoretical results. When $\xi = 10$ dB and $N_D = N_I \geq 2$, the difference between the two results increases. The reason is that the case with $\xi = 0$ dB corresponds to the EAP condition in which the theoretical PER does not include any approximations. As ξ or $f_D T$ increases, the theoretical PER becomes more inaccurate. This is because, for the UAP condition, $p_D(\dot{r}_D)$ of (24) and $p_I(\dot{r}_I)$ of (26) become more inaccurate as ξ or f_D increases. However, the discrepancy between the theoretical and simulation results is small, even when $N_D = N_I \geq 2$ and $\xi = 10$ dB.

Fig. 14 shows a plot of the theoretical PER versus α for the EAP condition, where $f_D = f_{DD} = f_{DI}$, and $f_D T = 0.20$. The PER appears to be insensitive to α, i.e., the PER performance of the ad hoc network is almost the same as the cellular system, although the double mobility causes faster fading. This case is because the PER only slightly increases with f_D, where $0.20 \leq f_D T \leq 0.20\sqrt{2}$, which can be observed in Fig. 9. Fig. 15 shows the effect of α on the theoretical PER for the UAP condition, where $\xi = 10$ dB, $f_D = f_{DD} = f_{DI}$, and $f_D T = 0.20$. It can be observed that the PER is also insensitive to α and the PER in the case where $N_D = N_I = 2$ becomes worse than for the EAP condition. This case is because, when ξ increases, the diversity effect is lost.

Note that the new Markov model is also useful for further analysis, considering upper layer protocols. For example, it has been applied to determine the optimal TCP/IP packet length for mobile communication systems [23].

In addition, note that the proposed Markov models are applicable to channel-coded systems. However, the application to channel-coded systems requires some modifications, which are explained as follows.

Let us consider channel coding that can correct at most e erroneous symbols of n coded symbols. The PER is equivalent to the probability that the number of erroneous symbols is greater than e. First, we assume that the symbol error does not occur only if the SIR or its lower bound is greater than λ_{th} during the symbol duration. Then, the aforementioned probability can be obtained using the proposed Markov model, which sets the time interval to the symbol duration.

IV. Conclusion

In this paper, we have derived two Markov models of the time-varying SIR over frequency-selective fading channels to analyze the PER of mobile radio communications under interference-dominant conditions. The two Markov models are first-order two-state for infinitesimal and finite time intervals. The state probabilities and the state transition probabilities were obtained from both the LCR and AOD of the fluctuating SIR, which can be determined based on a propagation model. It was also demonstrated that the LCR of the SIR becomes equivalent to the LCR of the SNR for a specific condition. The Markov model for the finite duration was used for the PER analysis. This analysis is valid not only for cellular communication systems but also for ad hoc mobile networks. The PER that was obtained from computer simulations agrees well with the theoretical PER when the average powers of both the desired and interfering signal components are equal—a condition that is referred to as the EAP condition. Even in other conditions, the simulation results agree with the theoretical results, which include an approximation. The analytical results also showed that the PER performance of ad hoc networks is almost the same as the PER of cellular systems, although faster fading is caused when both transmitters and receivers move around in ad hoc networks.

Appendix A
Derivation of (22)–(26)

Because r_D and r_I are statistically independent, $p(r_D, \dot{r}_D, r_I, \dot{r}_I)$ can be expressed as

$$p(r_D, \dot{r}_D, r_I, \dot{r}_I) = p(r_D, \dot{r}_D) p(r_I, \dot{r}_I). \tag{60}$$

We only have to derive $p(r_D, \dot{r}_D)$, because $p(r_I, \dot{r}_I)$ has the same mathematical form as that of $p(r_D, \dot{r}_D)$. $p(r_D, \dot{r}_D)$ can be rewritten as

$$p(r_D, \dot{r}_D) = p(\dot{r}_D|r_D)p(r_D) \tag{61}$$

where $p(\dot{r}_D|r_D)$ is the conditional probability density function of $\dot{r}_D$, given r_D. $p(r_D)$ and $p(\dot{r}_D|r_D)$ are derived as follows.

Derivation of $p(r_D)$: The joint probability density function $p(r_{Dl}, \dot{r}_{Dl})$ is given by [22]

$$p(r_{Dl}, \dot{r}_{Dl}) = p(r_{Dl})p(\dot{r}_{Dl}) \tag{62}$$

$$p(r_{Dl}) = \frac{r_{Dl}}{b_{Dl,0}} \exp\left(-\frac{r_{Dl}^2}{2b_{Dl,0}}\right) \tag{63}$$

$$p(\dot{r}_{Dl}) = \frac{1}{\sqrt{2\pi b_{Dl,2}}} \exp\left(-\frac{\dot{r}_{Dl}^2}{2b_{Dl,2}}\right). \tag{64}$$

Note that r_{Dl} and $\dot{r}_{Dl}$ are independent of each other and $\dot{r}_{Dl}$ is a Gaussian random variable with zero mean and variance $b_{Dl,2}$. $b_{Dl,2} = 2\pi^2(1+\alpha^2)f_{DD}^2 b_{Dl,0}$ and f_{DD} is the maximum Doppler frequency of the desired signals, which is derived from (13).

Let $p(\eta)$ be the probability density function of η, where $\eta = r_D^2 = \sum_{l=1}^{N_D} r_{Dl}^2$. The Laplace transform of $p(\eta)$ is equivalent to $\langle e^{-s\eta} \rangle$ and is thus given by

$$\begin{aligned}\int_0^\infty e^{-s\eta} p(\eta) d\eta &= \int_0^\infty dr_{D1} \cdots \int_0^\infty dr_{DN_D} \\ &\quad \times \exp\left(-s\sum_{l=1}^{N_D} r_{Dl}^2\right) p(r_{D1}, r_{D2}, \ldots, r_{DN_D}) \\ &= \prod_{l=1}^{N_D} \int_0^\infty dr_{Dl} \exp\left(-s r_{Dl}^2\right) p(r_{Dl}).\end{aligned} \tag{65}$$

Substituting (63) into (65) yields

$$\begin{aligned}\int_0^\infty e^{-s\eta} p(\eta) d\eta &= \prod_{l=1}^{N_D} \int_0^\infty dr_{Dl} \frac{r_{Dl}}{b_{Dl,0}} \\ &\quad \times \exp\left(-\frac{2b_{Dl,0}s+1}{2b_{Dl,0}} r_{Dl}^2\right) \\ &= \prod_{l=1}^{N_D} \frac{1}{2b_{Dl,0}s+1} \\ &= \begin{cases} (2b_{D0}s+1)^{-N_D}, & \text{for EAP} \\ \sum_{l=1}^{N_D} \frac{\pi_{Dl}}{2b_{Dl,0}s+1}, & \text{for UAP} \end{cases}\end{aligned} \tag{66}$$

where π_{Dl} is a constant that is defined by

$$\pi_{Dl} = \prod_{k=1, k\neq l}^{N_D} \frac{b_{Dl,0}}{b_{Dl,0} - b_{Dk,0}}. \tag{67}$$

The inverse Laplace transform of (66) is given by

$$p(\eta) = \begin{cases} \frac{1}{(N_D-1)!} \frac{\eta^{N_D-1}}{(2b_{D0})^{N_D}} \exp\left(-\frac{\eta}{2b_{D0}}\right), & \text{for EAP} \\ \sum_{l=1}^{N_D} \frac{\pi_{Dl}}{2b_{Dl,0}} \exp\left(-\frac{\eta}{2b_{Dl,0}}\right), & \text{for UAP.} \end{cases} \tag{68}$$

Based on the aforementioned equation and the definition $\eta = r_D^2$, $p(r_D)$ is derived as

$$\begin{aligned}p(r_D) &= p(\eta)\left|\frac{d\eta}{dr_D}\right| \\ &= \begin{cases} \frac{2}{(N_D-1)!} \frac{r_D^{2N_D-1}}{(2b_{D0})^{N_D}} \exp\left(-\frac{r_D^2}{2b_{D0}}\right), & \text{for EAP} \\ \sum_{l=1}^{N_D} \frac{\pi_{Dl} r_D}{b_{Dl,0}} \exp\left(-\frac{r_D^2}{2b_{Dl,0}}\right), & \text{for UAP.} \end{cases}\end{aligned} \tag{69}$$

Derivation of $p(\dot{r}_D|r_D)$: Let $\mathcal{R}_D = \{r_{Dl} | 1 \le l \le N_D\}$. $p(\dot{r}_D|r_D)$ is expressed as

$$\begin{aligned}p(\dot{r}_D|r_D) &= \int \cdots \int_{D(r_D)} p(\dot{r}_D, \mathcal{R}_D|r_D) \prod_{l=1}^{N_D} dr_{Dl} \\ &= \frac{1}{p(r_D)} \int \cdots \int_{D(r_D)} p(\dot{r}_D|\mathcal{R}_D, r_D) \\ &\quad \times p(\mathcal{R}_D, r_D) \prod_{l=1}^{N_D} dr_{Dl}\end{aligned} \tag{70}$$

where $D(r_D)$ is a domain of $\mathcal{R}_D$ that satisfies $(\sum_{l=1}^{N_D} r_{Dl}^2)^{1/2} = r_D$.

Differentiating $r_D = (\sum_{l=1}^{N_D} r_{Dl}^2)^{1/2}$ with respect to time yields

$$\dot{r}_D = \frac{2\sum_{l=1}^{N_D} r_{Dl}\dot{r}_{Dl}}{2\left(\sum_{l=1}^{N_D} r_{Dl}^2\right)^{1/2}} = \sum_{l=1}^{N_D} r_{Dl}\dot{r}_{Dl}/r_D. \tag{71}$$

Because $\dot{r}_{Dl}$ is a Gaussian random variable, $\dot{r}_D$ is equivalent to a linear combination of the Gaussian random variables, given $\mathcal{R}_D$. Thus, $\dot{r}_D$ is subject to the Gaussian distribution. Its mean value is equal to zero, because the mean value of $\{\dot{r}_{Dl} | 1 \le l \le N_D\}$ is zero, and its variance is given by

$$\left\langle \dot{r}_D^2 \right\rangle = \frac{\sum_{l=1}^{N_D} r_{Dl}^2 \left\langle \dot{r}_{Dl}^2 \right\rangle}{r_D^2} = \begin{cases} b_{D2}, & \text{for EAP} \\ \frac{\sum_{l=1}^{N_D} b_{Dl,2} r_{Dl}^2}{\sum_{l=1}^{N_D} r_{Dl}^2}, & \text{for UAP} \end{cases} \tag{72}$$

where $b_{D2} = 2\pi^2(1+\alpha^2)f_{DD}^2 b_{D0}$.

In the case of the UAP condition, $\langle \dot{r}_D^2 \rangle$ depends on $\mathcal{R}_D$, which makes $p(\dot{r}_D|r_D)$ very complicated. Thus, this variance

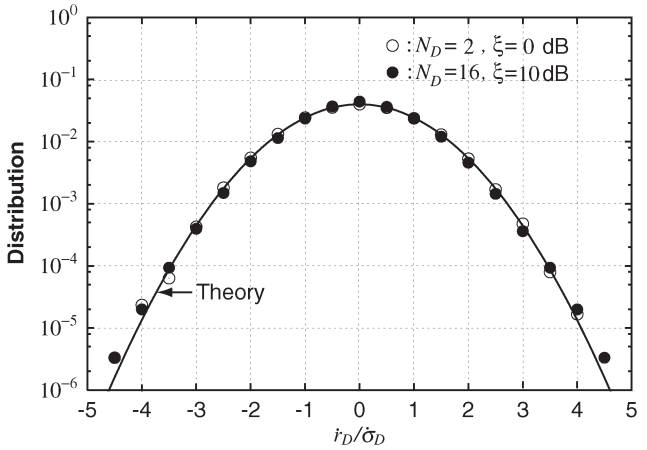

Fig. 16. Probability density function $p(\dot{r}_D)$.

is approximated as

$$\left\langle \dot{r}_D^2 \right\rangle \simeq \frac{\sum_{l=1}^{N_D} \left\langle r_{Dl}^2 \right\rangle b_{Dl,2}}{\sum_{l=1}^{N_D} \left\langle r_{Dl}^2 \right\rangle} = \frac{\sum_{l=1}^{N_D} b_{Dl,0} b_{Dl,2}}{\sum_{l=1}^{N_D} b_{Dl,0}} = \dot{\sigma}_D^2. \tag{73}$$

Because $\langle \dot{r}_D^2 \rangle$ does not depend on $\mathcal{R}_D$, even for the UAP condition, $\dot{r}_D$ becomes statistically independent of r_D and $\mathcal{R}_D$. Therefore, $p(\dot{r}_D|\mathcal{R}_D, r_D)$ is given by

$$\begin{aligned} p(\dot{r}_D|\mathcal{R}_D, r_D) &= p(\dot{r}_D) \\ &= \begin{cases} \frac{1}{\sqrt{2\pi b_{D2}}} \exp\left(-\frac{\dot{r}_D^2}{2b_{D2}}\right) & \text{for EAP} \\ \frac{1}{\sqrt{2\pi\dot{\sigma}_D^2}} \exp\left(-\frac{\dot{r}_D^2}{2\dot{\sigma}_D^2}\right) & \text{for UAP} \end{cases} \end{aligned} \tag{74}$$

and thus, $p(\dot{r}_D|r_D)$ of (70) can be expressed as

$$\begin{aligned} p(\dot{r}_D|r_D) &= \frac{p(\dot{r}_D)}{p(r_D)} \int \cdots \int_{D(r_D)} p(\mathcal{R}_D, r_D) \prod_{l=1}^{N_D} dr_{Dl} \\ &= \frac{p(\dot{r}_D)}{p(r_D)} p(r_D) = p(\dot{r}_D) \\ &= \begin{cases} \frac{1}{\sqrt{2\pi b_{D2}}} \exp\left(-\frac{\dot{r}_D^2}{2b_{D2}}\right), & \text{for EAP} \\ \frac{1}{\sqrt{2\pi\dot{\sigma}_D^2}} \exp\left(-\frac{\dot{r}_D^2}{2\dot{\sigma}_D^2}\right), & \text{for UAP.} \end{cases} \end{aligned} \tag{75}$$

To verify the approximation of (73), Fig. 16 compares $p(\dot{r}_D)$ of (75) with $p(\dot{r}_D)$ that was obtained by computer simulations. The simulation results were calculated from the number of times that $\dot{r}_D$ lies within $\dot{\sigma}_D/10$-long intervals. A path power ratio (in decibels) ξ is defined as $\xi = 10\log_{10}(b_{Dl,0}/b_{Dl+1,0})$, where $1 \le l \le N_D - 1$. Note that (75) is exact when $\xi = 0$ dB, which corresponds to the EAP condition. In Fig. 16, it is observed that differences between the simulation results and the theoretical values of (75) are negligible, even when $\xi = 10$ dB and $N_D = 16$.

$p(r_I, \dot{r}_I)$ is derived in the same way and expressed as

$$p(r_I, \dot{r}_I) = p(r_I)p(\dot{r}_I) \tag{76}$$

$$p(r_I) = \begin{cases} \frac{2}{(N_I-1)!} \frac{r_I^{2N_I-1}}{(2b_{I0})^{N_I}} \exp\left(-\frac{r_I^2}{2b_{I0}}\right), & \text{for EAP} \\ \sum_{m=1}^{N_I} \frac{\pi_{Im} r_I}{b_{Im,0}} \exp\left(-\frac{r_I^2}{2b_{Im,0}}\right), & \text{for UAP} \end{cases} \tag{77}$$

$$p(\dot{r}_I) = \begin{cases} \frac{1}{\sqrt{2\pi b_{I2}}} \exp\left(-\frac{\dot{r}_I^2}{2b_{I2}}\right), & \text{for EAP} \\ \frac{1}{\sqrt{2\pi\dot{\sigma}_I^2}} \exp\left(-\frac{\dot{r}_I^2}{2\dot{\sigma}_I^2}\right), & \text{for UAP} \end{cases} \tag{78}$$

where $b_{I2} = 2\pi^2(1+\alpha^2)f_{DI}^2 b_{I0}$, and $b_{Il,2} = 2\pi^2(1+\alpha^2)f_{DI}^2 b_{Il,0}$ when f_{DI} is the maximum Doppler frequency of the interfering signals. π_{Im} and $\dot{\sigma}_I^2$ are defined as

$$\pi_{Im} = \prod_{k=1, k\neq m}^{N_I} \frac{b_{Im,0}}{b_{Im,0} - b_{Ik,0}} \tag{79}$$

$$\dot{\sigma}_I^2 = \frac{\sum_{m=1}^{N_I} b_{Im,0} b_{Im,2}}{\sum_{m=1}^{N_I} b_{Im,0}}. \tag{80}$$

APPENDIX B
DERIVATION OF (34)

A of (32) can be rewritten as

$$A = I_1 - I_2 \tag{81}$$

$$I_1 = \int_{-\infty}^{\infty} d\dot{r}_D \dot{r}_D p_D(\dot{r}_D) \int_{-\infty}^{\lambda_{th}^{-1/2}\dot{r}_D} d\dot{r}_I p_I(\dot{r}_D) \tag{82}$$

$$I_2 = \lambda_{th}^{1/2} \int_{-\infty}^{\infty} d\dot{r}_D p_D(\dot{r}_D) \int_{-\infty}^{\lambda_{th}^{-1/2}\dot{r}_D} d\dot{r}_I \dot{r}_I p_I(\dot{r}_I). \tag{83}$$

EAP: Substituting (24) and (26) into (82) yields

$$\begin{aligned} I_1 &= \frac{1}{2\pi\sqrt{b_{D2}b_{I2}}} \int_{-\infty}^{\infty} d\dot{r}_D \dot{r}_D \exp\left(-\frac{\dot{r}_D^2}{2b_{D2}}\right) \\ &\quad \times \int_{-\infty}^{\lambda_{th}^{-1/2}\dot{r}_D} d\dot{r}_I \exp\left(-\frac{\dot{r}_I^2}{2b_{I2}}\right) \\ &= \frac{1}{2\pi\sqrt{b_{D2}b_{I2}}} \\ &\quad \times \left[-b_{D2}\exp\left(-\frac{\dot{r}_D^2}{2b_{D2}}\right) \int_{-\infty}^{\lambda_{th}^{-1/2}\dot{r}_D} d\dot{r}_I \exp\left(-\frac{\dot{r}_I^2}{2b_{I2}}\right)\right]_{-\infty}^{\infty} \\ &\quad + \frac{\lambda_{th}^{-1/2} b_{D2}}{2\pi\sqrt{b_{D2}b_{I2}}} \int_{-\infty}^{\infty} \exp\left(-\frac{\dot{r}_D^2}{2b_{D2}}\right) \exp\left(-\frac{\lambda_{th}^{-1}\dot{r}_D^2}{2b_{I2}}\right) d\dot{r}_D \end{aligned}$$

$$= \frac{\lambda_{th}^{-1/2} b_{D2}}{2\pi\sqrt{b_{D2}b_{I2}}} \int_{-\infty}^{\infty} \exp\left[-\left(\frac{b_{I2}+\lambda_{th}^{-1}b_{D2}}{2b_{D2}b_{I2}}\dot{r}_D^2\right)\right] d\dot{r}_D$$

$$= \frac{b_{D2}}{\sqrt{2\pi(b_{D2}+\lambda_{th}b_{I2})}}. \quad (84)$$

Similarly, substituting (24) and (26) into (83) gives

$$I_2 = \frac{\lambda_{th}^{1/2}}{2\pi\sqrt{b_{D2}b_{I2}}} \int_{-\infty}^{\infty} d\dot{r}_D \exp\left(-\frac{\dot{r}_D^2}{2b_{D2}}\right) \times \int_{-\infty}^{\lambda_{th}^{-1/2}\dot{r}_D} d\dot{r}_I \dot{r}_I \exp\left(-\frac{\dot{r}_I^2}{2b_{I2}}\right)$$

$$= \frac{\lambda_{th}^{1/2}}{2\pi\sqrt{b_{D2}b_{I2}}} \int_{-\infty}^{\infty} d\dot{r}_D \exp\left(-\frac{\dot{r}_D^2}{2b_{D2}}\right) \times \left[-b_{I2}\exp\left(-\frac{\dot{r}_I^2}{2b_{I2}}\right)\right]_{-\infty}^{\lambda_{th}^{-1/2}\dot{r}_D}$$

$$= -\frac{\lambda_{th}^{1/2}}{2\pi}\sqrt{\frac{b_{I2}}{b_{D2}}} \int_{-\infty}^{\infty} d\dot{r}_D \exp\left[-\left(\frac{b_{I2}+\lambda_{th}^{-1}b_{D2}}{2b_{D2}b_{I2}}\right)\dot{r}_D^2\right]$$

$$= -\frac{\lambda_{th}b_{I2}}{\sqrt{2\pi(b_{D2}+\lambda_{th}b_{I2})}}. \quad (85)$$

Thus, A of (81) is obtained as

$$A = \sqrt{\frac{b_{D2}+\lambda_{th}b_{I2}}{2\pi}}. \quad (86)$$

By substituting (23) and (25) into (33), B can be rewritten as

$$B = \frac{4\lambda_{th}^{\frac{2N_D-1}{2}}}{(N_D-1)!(N_I-1)!(2b_{D0})^{N_D}(2b_{I0})^{N_I}} \times \int_0^{\infty} r_I^{2N_D+2N_I-2}\exp\left(-\frac{b_{D0}+\lambda_{th}b_{I0}}{2b_{D0}b_{I0}}r_I^2\right) dr_I$$

$$= \frac{\pi^{1/2}(2N_D+2N_I-3)!!}{2^{N_D+N_I-3/2}(N_D-1)!(N_I-1)!} \times \frac{\lambda_{th}^{\frac{2N_D-1}{2}} b_{D0}^{\frac{2N_I-1}{2}} b_{I0}^{\frac{2N_D-1}{2}}}{(b_{D0}+\lambda_{th}b_{I0})^{(2N_D+2N_I-1)/2}} \quad (87)$$

where the following formula was used:

$$\int_0^{\infty} x^{2n}e^{-ax^2}dx = \frac{\pi^{1/2}(2n-1)!!}{2^{n+1}}a^{-\frac{2n+1}{2}} \quad (88)$$

with n and a being a positive integer and a positive real number, respectively.

Finally, substituting (86) and (87) into (31) yields

$$N_c = \frac{(2N_D+2N_I-3)!!}{2^{N_D+N_I-1}(N_D-1)!(N_I-1)!} \frac{\lambda_{th}^{\frac{2N_D-1}{2}} b_{D0}^{\frac{2N_I-1}{2}} b_{I0}^{\frac{2N_D-1}{2}} b_{t2}^{1/2}}{b_{t0}^{(2N_D+2N_I-1)/2}} \quad (89)$$

where $b_{t0} = b_{D0} + \lambda_{th}b_{I0}$, and $b_{t2} = b_{D2} + \lambda_{th}b_{I2}$.

UAP: With regard to UAP, A can be obtained by replacing b_{D2} and b_{I2} in (86) with $\dot{\sigma}_D^2$ and $\dot{\sigma}_I^2$, respectively. The result is given by

$$A = \sqrt{\frac{\dot{\sigma}_D^2+\lambda_{th}\dot{\sigma}_I^2}{2\pi}}. \quad (90)$$

By substituting (23) and (25) into (33), B can be rewritten as

$$B = \int_0^{\infty} dr_I \sum_{l=1}^{N_D} \frac{\pi_{Dl}\lambda_{th}^{1/2}r_I}{b_{Dl,0}} \exp\left(-\frac{\lambda_{th}r_I^2}{2b_{Dl,0}}\right) \times \sum_{m=1}^{N_I} \frac{\pi_{Im}r_I}{b_{Im,0}} \exp\left(-\frac{r_I^2}{2b_{Im,0}}\right)$$

$$= \lambda_{th}^{1/2} \sum_{l=1}^{N_D}\sum_{m=1}^{N_I} \frac{\pi_{Dl}\pi_{Im}}{b_{Dl,0}b_{Im,0}} \times \int_0^{\infty} dr_I r_I^2 \exp\left[-\left(\frac{b_{Dl,0}+\lambda_{th}b_{Im,0}}{2b_{Dl,0}b_{Im,0}}\right)r_I^2\right]. \quad (91)$$

Using (88), B of (91) is calculated as

$$B = \frac{\lambda_{th}^{1/2}\pi^{1/2}}{2^{1/2}} \sum_{l=1}^{N_D}\sum_{m=1}^{N_I} \frac{\pi_{Dl}\pi_{Im}(b_{Dl,0}b_{Im,0})^{1/2}}{(b_{Dl,0}+\lambda_{th}b_{Im,0})^{3/2}}. \quad (92)$$

Finally, substituting (90) and (92) into (31) yields

$$N_c = \frac{\lambda_{th}^{1/2}\left(\dot{\sigma}_D^2+\lambda_{th}\dot{\sigma}_I^2\right)^{1/2}}{2} \times \sum_{l=1}^{N_D}\sum_{m=1}^{N_I} \frac{\pi_{Dl}\pi_{Im}(b_{Dl,0}b_{Im,0})^{1/2}}{(b_{Dl,0}+\lambda_{th}b_{Im,0})^{3/2}}. \quad (93)$$

APPENDIX C
DERIVATION OF (41)

P_l of (40) can be expressed as

$$P_l = \int_0^{\infty} dr_I p_I(r_I) C(r_I) \quad (94)$$

$$C(r_I) = \int_0^{\lambda_{th}^{1/2}r_I} p_D(r_D) dr_D. \quad (95)$$

EAP: Substituting (23) into (95) yields

$$C(r_I) = \frac{2}{(N_D-1)!(2b_{D0})^{N_D}} \times \int_0^{\lambda_{th}^{1/2}r_I} {r_D}^{2N_D-1}\exp\left(-\frac{r_D^2}{2b_{D0}}\right) dr_D. \quad (96)$$

To obtain $C(r_I)$, $a(x,n)$ is defined as

$$a(x,n) = \int_0^x y^{2n+1} \exp(-\beta y^2) dy \tag{97}$$

where n is a nonnegative integer, and β is a positive real number.

A recursive form of $a(x,n)$ is given by

$$\begin{aligned} a(x,n) &= -y^{2n} \frac{e^{-\beta y^2}}{2\beta}\bigg|_0^x + \int_0^x 2ny^{2n-1} \frac{e^{-\beta y^2}}{2\beta} dy \\ &= -\frac{x^{2n} e^{-\beta x^2}}{2\beta} + \frac{n a(x,n-1)}{\beta}. \end{aligned} \tag{98}$$

Repeatedly using this recursive form, $a(x,n)$ can be expressed as

$$\begin{aligned} a(x,n) &= -\frac{x^{2n} e^{-\beta x^2}}{2\beta} \\ &\quad + \frac{n}{\beta}\left[-\frac{x^{2(n-1)} e^{-\beta x^2}}{2\beta} + \frac{(n-1)a(x,n-2)}{\beta} \right] \\ &= -\frac{e^{-\beta x^2}}{2\beta} \sum_{k=0}^{n-1} \frac{n!}{(n-k)!} \frac{x^{2(n-k)}}{\beta^k} + \frac{n!}{\beta^n} a(x,0). \end{aligned} \tag{99}$$

$a(x,0)$ is calculated as

$$a(x,0) = \int_0^x y \exp(-\beta y^2) dy = -\frac{e^{-\beta y^2}}{2\beta}\bigg|_0^x = \frac{1 - e^{-\beta x^2}}{2\beta}. \tag{100}$$

Substituting (100) into (99) yields

$$a(x,n) = \frac{n!}{2\beta^{n+1}} - \frac{x^{2n} e^{-\beta x^2}}{2\beta} \sum_{k=0}^{n} \frac{n!}{(n-k)!} (\beta x^2)^{-k}. \tag{101}$$

Using $a(\lambda_{th}^{1/2} r_I, N_D - 1)$, with β being $(2b_{D0})^{-1}$, $C(r_I)$ of (96) can be expressed as

$$\begin{aligned} C(r_I) &= \frac{2a\left(\lambda_{th}^{1/2} r_I, N_D - 1\right)}{(N_D-1)!(2b_{D0})^{N_D}} \\ &= 1 - \frac{\lambda_{th}^{N_D-1}}{(2b_{D0})^{N_D-1}} \exp\left(-\frac{\lambda_{th} r_I^2}{2b_{D0}}\right) \\ &\quad \times \sum_{k=0}^{N_D-1} \left(\frac{2b_{D0}}{\lambda_{th}}\right)^k \frac{r_I^{2(N_D-1-k)}}{(N_D-1-k)!} \end{aligned} \tag{102}$$

where (101) was used.

The substitution of (102) and (25) into (94) and the use of (40) yield P_u as

$$\begin{aligned} P_u &= \frac{2}{(N_I-1)!(2b_{I0})^{N_I}} \frac{\lambda_{th}^{N_D-1}}{(2b_{D0})^{N_D-1}} \\ &\quad \times \sum_{k=0}^{N_D-1} \frac{1}{(N_D-1-k)!} \left(\frac{2b_{D0}}{\lambda_{th}}\right)^k \\ &\quad \times \int_0^\infty r_I^{2(N_D+N_I-k)-3} \exp\left(-\frac{b_{D0} + \lambda_{th} b_{I0}}{2b_{D0} b_{I0}} r_I^2\right) dr_I. \end{aligned} \tag{103}$$

Using (101), P_u of (103) is given by

$$\begin{aligned} P_u &= \left(\frac{b_{D0}}{b_{t0}}\right)^{N_I} \\ &\quad \times \sum_{k=0}^{N_D-1} \binom{N_D + N_I - k - 2}{N_I - 1} \left(\frac{\lambda_{th} b_{I0}}{b_{t0}}\right)^{N_D-k-1}. \end{aligned} \tag{104}$$

UAP: Substituting (23) into (95) yields

$$\begin{aligned} C(r_I) &= \sum_{l=1}^{N_D} \frac{\pi_{Dl}}{b_{Dl,0}} \int_0^{\lambda_{th}^{1/2} r_I} r_D \exp\left(-\frac{r_D^2}{2b_{Dl,0}}\right) dr_D \\ &= \sum_{l=1}^{N_D} \pi_{Dl} \left[1 - \exp\left(-\frac{\lambda_{th} r_I^2}{2b_{Dl,0}}\right)\right]. \end{aligned} \tag{105}$$

Using (105) and (25), P_l of (94) is given by

$$\begin{aligned} P_l &= \sum_{l=1}^{N_D} \pi_{Dl} \sum_{m=1}^{N_I} \frac{\pi_{Im}}{b_{Im,0}} \\ &\quad \times \int_0^\infty r_I \left[1 - \exp\left(-\frac{\lambda_{th} r_I^2}{2b_{Dl,0}}\right)\right] \exp\left(-\frac{r_I^2}{2b_{Im,0}}\right) dr_I \\ &= \sum_{l=1}^{N_D} \pi_{Dl} \sum_{m=1}^{N_I} \frac{\pi_{Im}}{b_{Im,0}} \\ &\quad \times \Bigg\{ \left[-b_{Im,0} \exp\left(-\frac{r_I^2}{2b_{Im,0}}\right)\right]_0^\infty \\ &\qquad - \Bigg[-\frac{b_{Dl,0} b_{Im,0}}{b_{Dl,0} + \lambda_{th} b_{Im,0}} \\ &\qquad\quad \times \exp\left(-\frac{b_{Dl,0} + \lambda_{th} b_{Im,0}}{2b_{Dl,0} b_{Im,0}} r_I^2\right) \Bigg]_0^\infty \Bigg\} \\ &= \sum_{l=1}^{N_D} \pi_{Dl} \left(\sum_{m=1}^{N_I} \pi_{Im} - \sum_{m=1}^{N_I} \frac{\pi_{Im} b_{Dl,0}}{b_{Dl,0} + \lambda_{th} b_{Im,0}} \right). \end{aligned} \tag{106}$$

Because $\sum_{l=1}^{N_D} \pi_{Dl} = \sum_{m=1}^{N_I} \pi_{Im} = 1$, P_u in (40) is obtained as

$$P_u = \sum_{l=1}^{N_D} \sum_{m=1}^{N_I} \frac{\pi_{Dl} \pi_{Im} b_{Dl,0}}{b_{Dl,0} + \lambda_{th} b_{Im,0}}. \tag{107}$$

ACKNOWLEDGMENT

The authors would like to thank the anonymous reviewers for their insightful comments, which provided valuable guidance as to how this paper could be improved.

REFERENCES

[1] M. Taferner and E. Bonek, *Wireless Internet Access Over GSM and UMTS*. New York: Springer-Verlag, 2002.

[2] C. H. C. Leung, Y. Kikumoto, and S. A. Sorensen, "The throughput efficiency of the Go-Back- N ARQ scheme under Markov and related error structures," *IEEE Trans. Commun.*, vol. 36, no. 2, pp. 231–234, Feb. 1988.

[3] S. R. Kim and C. K. Un, "Throughput analysis for two ARQ schemes using combined transition matrix," *IEEE Trans. Commun.*, vol. 40, no. 11, pp. 1679–1683, Nov. 1992.

[4] T. Sato, M. Kawabe, T. Kato, and A. Fukasawa, "Throughput analysis method for hybrid ARQ schemes over burst error channels," *IEEE Trans. Veh. Technol.*, vol. 42, no. 1, pp. 110–118, Feb. 1993.

[5] H. S. Wang and P. C. Chang, "On verifying the first-order Markovian assumption for a Rayleigh fading channel model," *IEEE Trans. Veh. Technol.*, vol. 45, no. 2, pp. 353–357, May 1996.

[6] M. Zorzi, R. R. Rao, and L. B. Milstein, "ARQ error control for fading mobile radio channels," *IEEE Trans. Veh. Technol.*, vol. 46, no. 2, pp. 445–455, May 1997.

[7] H. S. Wang and N. Moayeri, "Finite-state Markov model—A useful model for radio communication channels," *IEEE Trans. Veh. Technol.*, vol. 44, no. 1, pp. 163–171, Feb. 1995.

[8] Q. Zhang and S. A. Kassam, "Finite-state Markov model for Rayleigh fading channels," *IEEE Trans. Commun.*, vol. 47, no. 11, pp. 1688–1692, Nov. 1999.

[9] F. Babich and G. Lombardi, "A Markov model for the mobile propagation channel," *IEEE Trans. Veh. Technol.*, vol. 49, no. 1, pp. 63–73, Jan. 2000.

[10] C. C. Tan and N. C. Beaulieu, "On first-order Markov modeling for the Rayleigh fading channel," *IEEE Trans. Commun.*, vol. 48, no. 12, pp. 2032–2040, Dec. 2000.

[11] L. Yang and M. S. Alouini, "Average outage duration of multiuser wireless communication systems with a minimum signal power requirement," in *Proc. IEEE Veh. Tech. Conf.*, May 2002, pp. 1507–1511.

[12] Y. C. Ko, M. R. Burr, M. S. Alouini, and A. Abdi, "Average outage duration of interference-limited wireless communication systems," in *Proc. IEEE Veh. Tech. Conf.*, May 2002, pp. 1284–1288.

[13] L. Yang and M. S. Alouini, "On the average outage rate and average outage duration of wireless communication systems with multiple cochannel interferers," *IEEE Trans. Wireless Commun.*, vol. 3, no. 4, pp. 1142–1153, Jul. 2004.

[14] L. Yang and M. S. Alouini, "Performance comparison of different selection combining algorithms in the presence of cochannel interference," *IEEE Trans. Veh. Technol.*, vol. 55, no. 2, pp. 559–571, Mar. 2006.

[15] F. Babich, F. Santucci, and F. Graziosi, "Modeling of power-controlled interference-limited wireless channels," in *Proc. 5th WPMC*, Oct. 2002, vol. 3, pp. 941–945.

[16] F. Babich, F. Santucci, and F. Graziosi, "Performance of error control schemes for fading channels with power control and MAI," in *Proc. IEEE Veh. Tech. Conf.*, May 2004, pp. 318–322.

[17] A. Fahmer and U. Fecker, "Markov chain models for the investigation of fast power control for FDD-UMTS," in *Proc. Pers. Mobile Commun. Conf.*, Apr. 2003, pp. 565–569.

[18] L. Zheng, H. Yousefi'zadeh, and H. Jafarkhani, "Resource allocation in fading wireless ad hoc networks with temporally correlated loss," in *Proc. IEEE Wireless Commun. Netw. Conf.*, Mar. 2004, vol. 3, pp. 1341–1346.

[19] R. Wang and D. C. Cox, "Channel modeling for ad hoc mobile wireless networks," in *Proc. IEEE Veh. Tech. Conf.*, May 2002, pp. 21–25.

[20] Y. Tateishi, K. Fukawa, and H. Suzuki, "Analysis of packet transmission for ad hoc mobile wireless networks," in *Proc. IEEE Veh. Tech. Conf.*, Apr. 2003, pp. 1233–1237.

[21] J. G. Proakis, *Digital Communications*, 3rd ed. New York: McGraw-Hill, 1995.

[22] W. C. Jakes, Jr., *Microwave Mobile Communications*. Hoboken, NJ: Wiley, 1974.

[23] K. Fukawa, S. Motoyama, and H. Suzuki, "Markov model analysis on the optimal TCP/IP packet length in mobile communication systems," in *Proc. 6th WPMC*, Oct. 2003, pp. 318–322.

Kazuhiko Fukawa (M'12) received the B.S. and M.S. degrees in physics and the Dr. Eng. degree in electrical and electronics engineering from Tokyo Institute of Technology, Tokyo, Japan, in 1985, 1987, and 1998, respectively.

In 1987, he joined the Nippon Telegraph and Telephone Corporation (NTT), Kanagawa, Japan. Since then, he has been engaged in research on digital mobile radio communication systems and applications of the adaptive signal processing, including adaptive equalization, interference cancellation, and adaptive arrays. From 1994 to 2000, he was a Senior Research Engineer with the NTT Mobile Communications Network Inc. (NTT DoCoMo), Kanagawa. Since April 2000, he has been an Associate Professor with the Department of Communications and Integrated Systems, Tokyo Institute of Technology.

Dr. Fukawa is a member of the Institute of Electronics, Information, and Communication Engineers (IEICE) of Japan. He received the Best Paper Award from IEICE in 1995, 2007, 2009, and 2012, the Best Paper Prize from the European Wireless Technology Conference, and the Achievement Award from IEICE in 2009.

Hiroshi Suzuki (M'78) received the B.S. degree in electrical engineering, the M.S. degree in physical electronics, and the Dr. Eng. degree in electrical and electronics engineering from Tokyo Institute of Technology, Tokyo, Japan, in 1972, 1974, and 1986, respectively.

In 1974, he joined the Electrical Communication Laboratories, Nippon Telegraph and Telephone Corporation (NTT), Kanagawa, Japan, where he was engaged in research on devices in millimeter-wave regions. Since 1978, he has been engaged in fundamental and developmental research on digital mobile communication systems. From 1992 to 1996, he was an Executive Research Engineer with the Research and Development Department, NTT Mobile Communications Network Inc. (NTT DoCoMo), Kanagawa. Since September 1996, he has been a Professor with the Department of Communications and Integrated Systems, Tokyo Institute of Technology. His research interests include various applications of the adaptive signal processing to radio signal transmission, particularly adaptive arrays, multiuser detection, interference canceling, and multiple-input–multiple-output–orthogonal frequency-division multiplexing for future advanced multiple access communication systems.

Dr. Suzuki is a member of the Institute of Electronics, Information, and Communication Engineers (IEICE) of Japan. He received the Best Paper Award from the IEICE in 1995, 2007, 2009, and 2012 at the European Wireless Technology Conference in 2009, the Fellowship Award from IEICE in 2006, and the IEICE Achievement Award in 2009.

Yumiko Tateishi received the B.S. degree in computer science and the M.S. degree in computational intelligence and systems science from Tokyo Institute of Technology, Tokyo, Japan, in 2003 and 2005, respectively.

She is currently with the Department of Computational Intelligence and Systems Science, Tokyo Institute of Technology, Kanagawa, Japan. Her research interests include neural network and neural mechanisms.

Ms. Tateishi is a member of the Institute of Electronics, Information, and Communication Engineers of Japan.